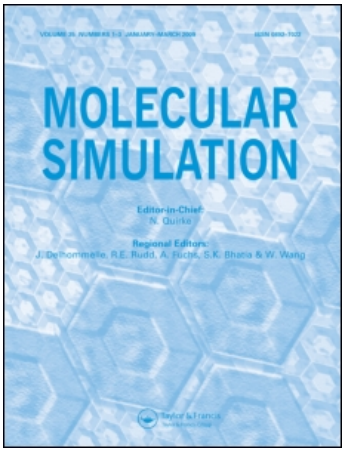

Molecular Simulation
Publication details, including instructions for authors and subscription information:
http://www.informaworld.com/smpp/title~content=t713644482

Molecular Dynamics Simulation of Two Dimensional Flow Past a Plate

S. T. Cui[a]; Denis J. Evans[a]
[a] Research School of Chemistry, The Australian National University, Canberra, Australia

To cite this Article Cui, S. T. and Evans, Denis J.(1992) 'Molecular Dynamics Simulation of Two Dimensional Flow Past a Plate', Molecular Simulation, 9: 3, 179 — 192
To link to this Article: DOI: 10.1080/08927029208047425
URL: http://dx.doi.org/10.1080/08927029208047425

Molecular Simulation, 1992, Vol. 9, pp. 179–192
Reprints available directly from the publisher
Photocopying permitted by license only

MOLECULAR DYNAMICS SIMULATION OF TWO DIMENSIONAL FLOW PAST A PLATE

S.T. CUI and DENIS J. EVANS

Research School of Chemistry, The Australian National University, GPO Box 4, Canberra, ACT 2601, Australia

(*Received March 1992, accepted April 1992*)

We describe molecular dynamics simulations of ~ 50,000 disks flowing past a plate. The simulations were performed using an algorithm which improves the velocity and temperature stability of the inlet fluid stream. At Reynolds numbers of ~ 30 and ~ 60, vortices were observed to alternately peel off the two edges of the plate. At a Reynolds number of ~ 15, the flow showed the laminar flow behaviour. We measured the drag coefficient of the plate as a function of Reynolds number and describe the spatial/temporal variation of local thermodynamic variables, (i.e. density, temperature and pressure). Relatively low values of the local density and temperature were found to correspond with the centers of the vortices. In spite of relatively large variations in temperature and density in the down stream fluid, local thermodynamic equilibrium was satisfied with considerable accuracy at all positions in the system.

KEY WORDS: Two dimensional flow, Reynolds number, plate drag coefficient

INTRODUCTION

Recently atomistic simulations have revealed a variety of complex hydrodynamic phenomena. These phenomena had previously only been studied theoretically using macroscopic equations such as the Navier–Stokes equation. These new molecular dynamics simulations have revealed that in small systems of typically less than 100,000 atoms, one can observe the formation of vortices in flow past a plate [1] and flow past a cylinder [2]. Perhaps even more surprisingly one can observe Rayleigh–Bénard instabilities [3, 4] in molecular dynamics simulations of only a few thousand particles.

This work is to be contrasted with another new computer simulation technique namely Lattice Gas Cellular Automata (LGCA) [5]. The latter replaces atoms that interact via short ranged atomic force fields and evolve in time according to the deterministic Newtonian equations of motion with a dynamical lattice gas that evolves in discrete time.

There are some important differences between the molecular dynamics approach which employs continuous space/time coordinates and deterministic equations of motion and the discrete LGCA models which are usually stochastic. Currently LGCA are only capable of describing incompressible flows. This means that comparisons with experiment are restricted to the low Mach number regime. This is in spite of the fact that in the LGCA simulations the Mach number is often quite high — in order to achieve high Reynolds numbers. (The Reynolds number, R_e, is defined as, $R_e = \rho v l/\eta$, where ρ is the density, v the flow velocity, l the characteristic length of an obstacle, and η the viscosity of the fluid.)

In molecular dynamics the same Reynolds/Mach number constraints apply. For a given system size one tries to maximize the Reynolds number while maintaining the Mach number less than unity. However in molecular dynamics simulations the system is far more realistic and the flows are observed to be highly anisochoric and non isothermal. One of the aims of this paper is to observe the temperature, density and pressure variations that are found in these small simulations of "macroscopic" flows.

Following References 1 and 2, we report the results of molecular dynamics simulation of flow past a plate in two dimensions. Besides providing further evidence of continuous vortex shedding behavior, our simulation examines the degree to which local thermodynamic equilibrium is satisfied within the shedding vortices themselves. The influence of Reynolds number on flow characteristics is studied, and an attempt is made to study the variation of drag coefficient with Reynolds number.

In comparison to Reference 1, which also studied flow past a plate, we use a continuous WCA potential rather than a hard sphere potential and we study a liquid like, rather than gas like, density. Although our fluid was similar to that studied in Reference 2, we consider flow past a plate rather than flow past a disk. We also introduce improved techniques for controlling the inlet flow conditions (i.e., the temperature, density and flow velocity of the input fluid stream).

THE MODEL

The system we studied consisted of 49,804 particles in two dimensions. The interaction potential among the particles is the WCA potential,

$$\phi = \begin{cases} 4\varepsilon\left[\left(\frac{\sigma}{r}\right)^{12} - \left(\frac{\sigma}{r}\right)^{6}\right] + 1 & r \leqslant 2^{1/6} \\ 0 & r > 2^{1/6} \end{cases} \tag{1}$$

All units for the calculations and the description of results are reduced to dimensionless form using the WCA potential parameters ε, σ as the energy and length units and the particle mass m, as the mass unit. Initially 51,200 particles were placed on a regular triangular lattice within a rectangle with a height to width ratio, L_y/L_x, of 1/4. The cell height L_y, was determined from the relation $L_y = (0.25N/\rho)^{1/2}$ and the density, ρ, was fixed at 0.75. The length of the obstructing plate was $L_y/2$ and it was oriented at 45° to the flow direction, namely x. The lower end of the plate was $3/8L_x$ from the leftmost cell boundary and its y position is such that the center of the plate was at $L_y/2$.

WCA walls were used at the two y boundaries and periodic boundary conditions used at the x boundaries. The interaction between the particles and either the walls or the plate was mediated by the WCA potential, with the particle-particle separation, r, in Equation (1) replaced by the shortest distance between the particle and the wall or the plate.

At the beginning of the simulation all the particles within the cutoff distance of both the plate and the walls were removed. This reduced the actual total number of particles to 49,804, resulting in an actual density of $0.73 \leqslant \rho \leqslant 0.75$. In the absence of any global flow, the system was allowed to relax to equilibrium.

In order to initiate continuous flow around the obstructing plate, the desired average flow velocity was added to the equilibrated random particle velocities of each particle. Because of the periodic boundaries, particles flowing out of the simulation

cell through the right x-face re-enter through the leftmost face of the simulation cell. This is essentially the Meiburg algorithm of Reference 1.

With the passage of time such a flow will gradually slow down with streaming kinetic energy being converted into heat. In order to maintain the flow at constant average velocity and inlet temperature, we designed an algorithm in which the simulation cell is similar to a recirculating wind tunnel. When the right most particles exit and re-enter at the left face they pass through two *conditioning* zones which reset the momentum and the temperature of the inlet fluid. A two stage conditioning process consisting of both stochastic and deterministic stages was found to produce noticeably better results than those from a single stage process such as the one used for example in Reference [2].

The system consisted of three different regions. On the leftmost x-face of the system there is a very thin stochastic thermostatting region, Q. This region contains less than ~ 100 particles. The total x-momentum of particles in Q is unaltered. The total y-momentum is constrained to be zero. A stochastic Andersen thermostat helps to reset the temperature of the Q-region to the desired value.

Further to the right is a small thermostat region, R, consisting of $\sim 1/10$ of the total simulation volume. In this region a Nosé–Hoover deterministic thermostat [6] was used to reset the temperature and an external field was applied to particles in R to ensure that the total x-momentum of *all* the fluid particles was constant.

Further still to the right was the free flow region, S, in which the fluid particles interacted with the obstructing plate before flowing further to the right and eventually re-entering the left face of the "wind tunnel" once again. In S the particles evolve in time according to Newton's laws interacting only with each other, with the side walls and with the obstructing plate. Inside S, there are no thermostats or external fields which effect the motion of the fluid particles.

The equations of motion for particles in R or S were

$$\begin{aligned} \dot{\mathbf{q}}_i &= \frac{\mathbf{p}_i}{m} \\ \dot{\mathbf{p}}_i &= \mathbf{F}_i - \left[\frac{F_p}{N_R} \hat{\mathbf{x}} + \alpha(\mathbf{p}_i - \mathbf{p}_R) \right] S_i \\ \dot{\alpha} &= \frac{1}{\tau^2} \left(\frac{T_R}{T_0} - 1 \right) \end{aligned} \tag{2}$$

Where $S_i = 1$ if particle i is in the region R and is zero otherwise. T_0 is the desired temperature, chosen to be 1.0 in the simulation. The Nosé–Hoover time constant, τ^2 was chosen to be 0.05. The force, $\mathbf{F}_i$, is the total force on particle i due to the other atoms and any possible wall or plate interactions. (In the very thin stochastic region, Q, a stochastic Andersen thermostat was employed rather than the deterministic Nosé–Hoover thermostat used in R.)

The instantaneous temperature of the thermostatting region T_R, is defined by

$$T_R = \frac{1}{(N_R - 1)k_B} \sum_{i \in R} \frac{1}{m} (\mathbf{p}_i - \mathbf{p}_R)^2 \tag{3}$$

where

$$N_R = \sum_{i=1}^{N} S_i = \sum_{i \in R} 1 \tag{4}$$

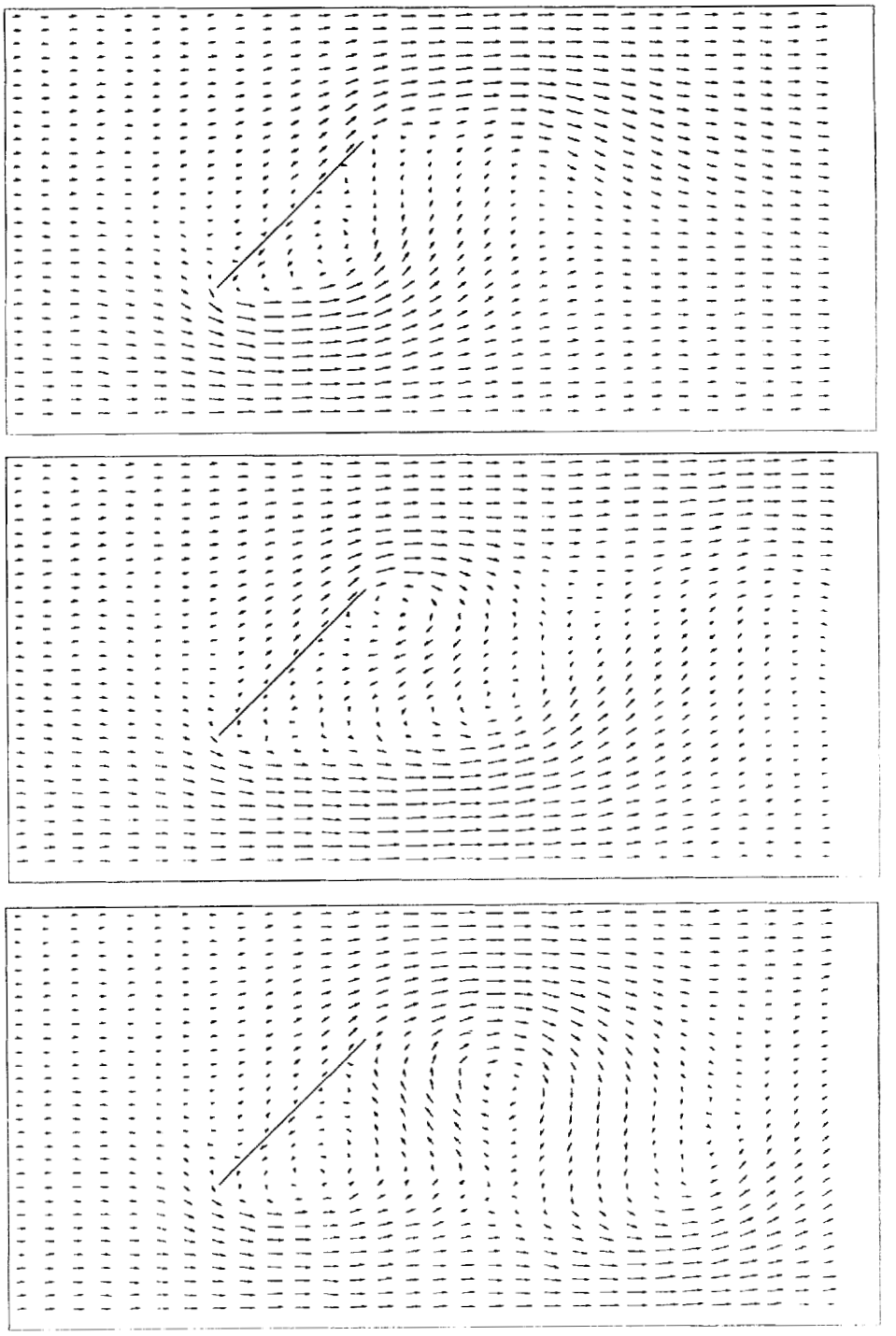

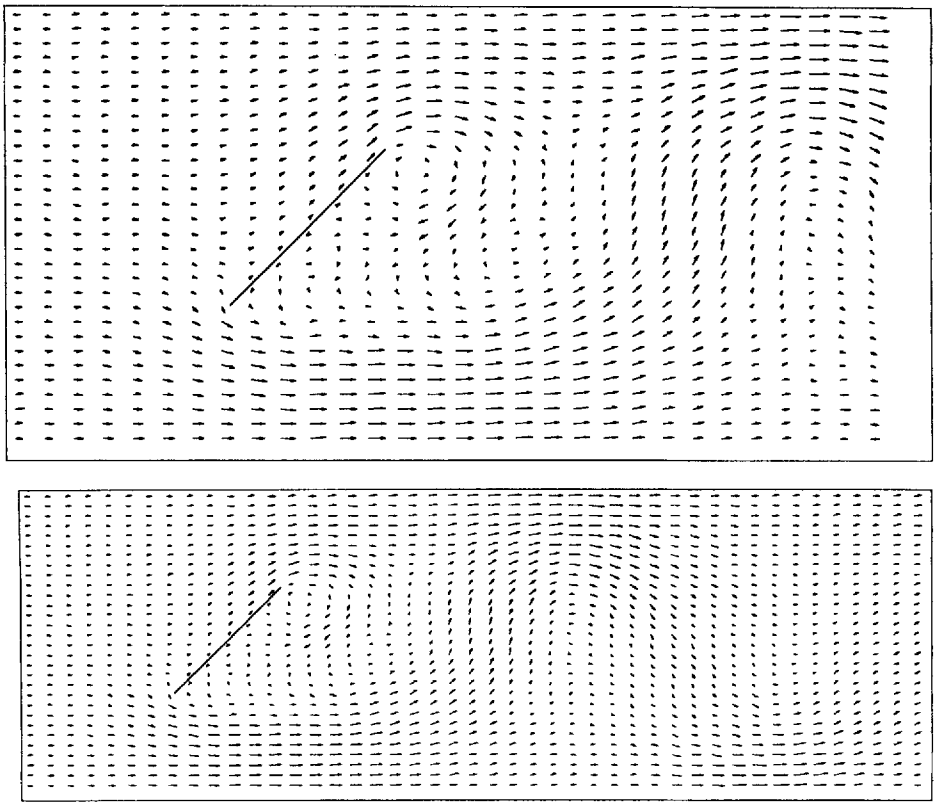

Figure 1 Shows the sequence of velocity fields at different times for flow velocity 2.0. (a) $t = 42$; (b) $t = 84$; (c) $t = 126$; (d) $t = 186$. (e) The velocity field for the right three quarters of the system at $t = 186$.

is the number of particles in the thermostat region, R. $\mathbf{p}_R$ is the average momentum per particle inside R.

In Equation (2), F_p is the x-component of the total force exerted on the particles by the plate. Thus the term involving F_p, in Equation (2) ensures that the total x-component of momentum of the system is held constant.

To calculate local thermodynamic properties such as the temperature we divided the whole system into 120 × 30 equal sized square cells. In each cell, β, we compute the average flow velocity, $\mathbf{u}_\beta$, from the equation,

$$\mathbf{u}_\beta = \frac{\sum_{i \in \mathbf{b}} \mathbf{p}_i}{\sum_{i \in \beta} m} \tag{5}$$

If N_β is the number of particles in cell β, the temperature, T_β, of cell β is calculated from the equation,

$$(N_\beta - 1)k_B T_\beta = \sum_{i \in \beta} \frac{(\mathbf{p}_i - m\mathbf{u}_\beta)^2}{2m} \tag{6}$$

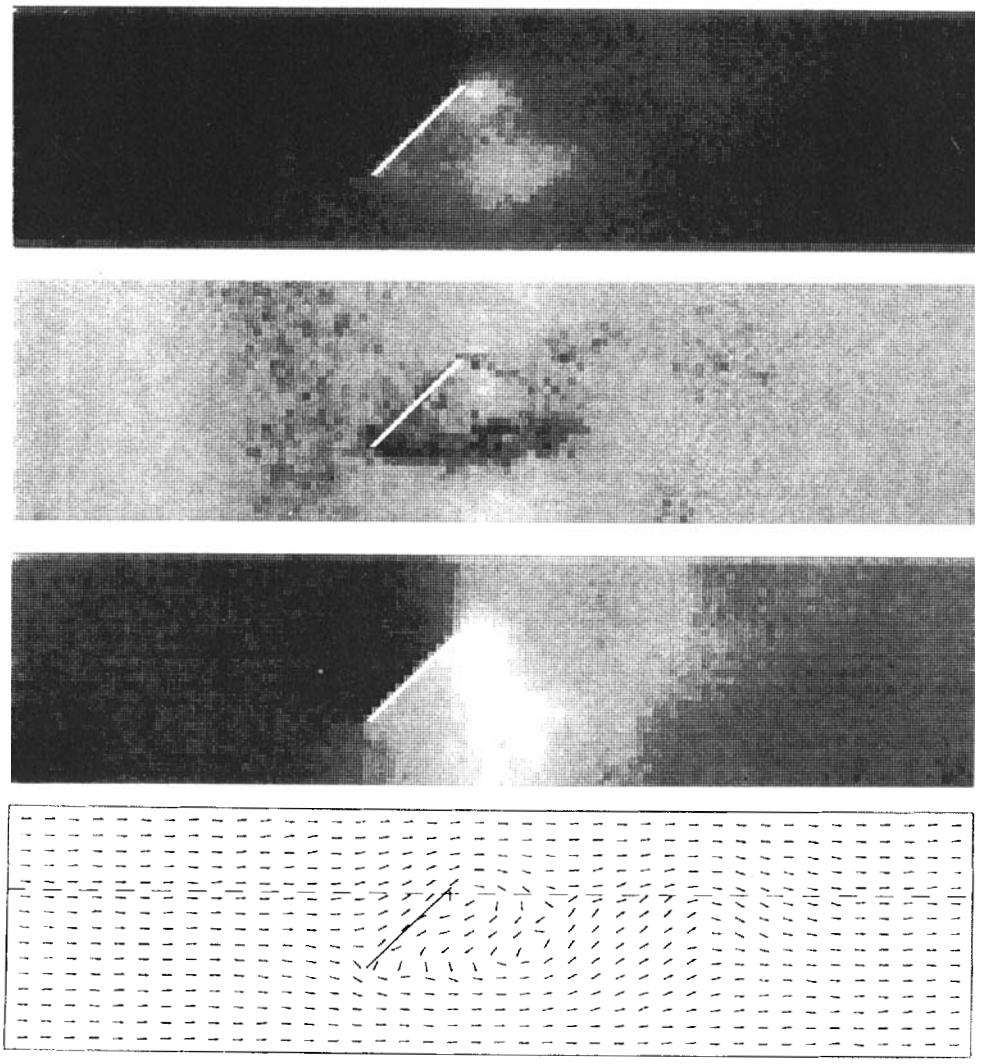

Figure 2 (a) From top to bottom we show the local distributions of the density, temperature and pressure at $t = 84$ as represented on a 256 color gray scale image with darker color representing higher numerical values. (b) Plots show the respective numerical values of the density, temperature and pressure along the ruled horizontal line shown in (a), all quantities are in MD units. (c) The same distributions as in (a), but at a later time, $t = 186$. (d) The same plots as in (b), corresponding to the distributions in (c). The crosses in the pressure plot indicate the equilibrium pressure as determined from the independent equilibrium simulation for 224 particles.

The main elements of our algorithm are clear. As fluid particles flow through the system with their periodic images re-entering at the left x-face of the simulation cell, the particles enter a thermostatting region. In this region their temperature is re-set to the desired value. Also within the thermostatting region a force is imposed on the fluid particles which ensures that the total x component of momentum of the system

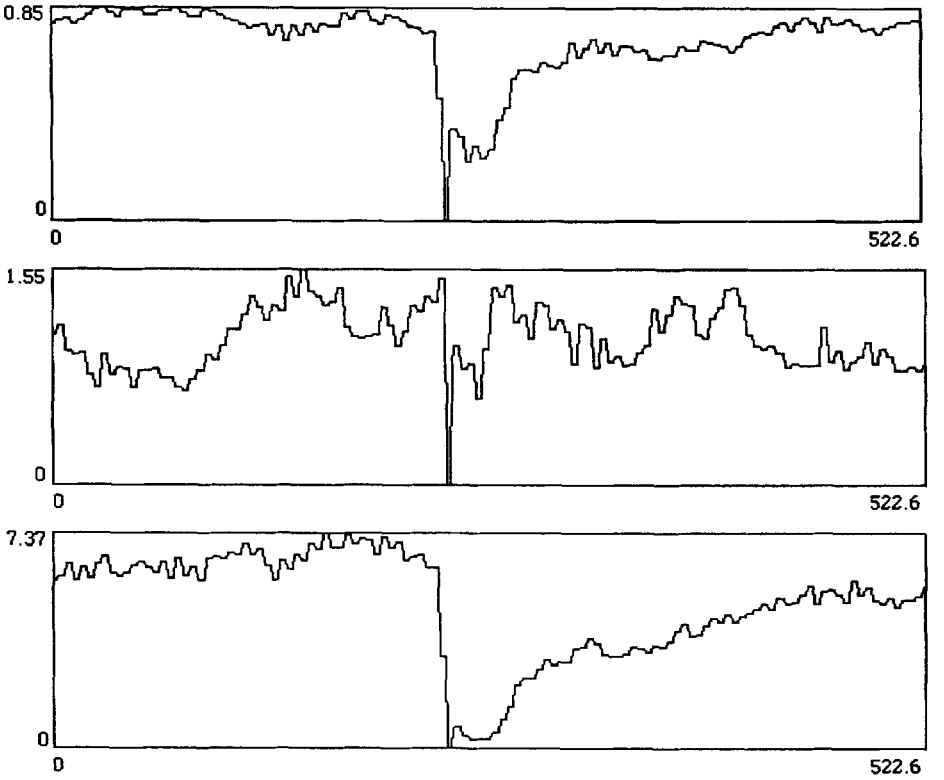

Figure 2 Continued. (b)

is constant. To start the "wind tunnel" into operation one simply adds some momentum at $t = 0$, to each particle and then watches the flow evolve. To the right of the thermostatting region the particles evolve in time according to Newton's laws interacting only with each other and with the obstructing plate. Outside R and Q, there are no thermostats or external fields which alter the motion of the fluid particles.

This algorithm has a distinct advantage over the Rapaport algorithm of Reference [2] where the thermostatting is performed stochastically as re-entering particles cross the left x-face of the simulation cell and where a homogeneous "gravitional" field acts on *all* the particles in order to generate a flow. Without knowing the friction coefficient in advance it is impossible to know how large to make the field in order to generate a required flow velocity.

A minor variation that can be used to increase the inlet stability for high flow rates is to set $\mathbf{p}_R$ in Equation (2) to be equal to $m\mathbf{u}_0$, where $\mathbf{u}_0$ is the desired flow velocity. This was done in the case of an initial flow velocity of 2.0.

RESULTS

We studied the behaviour of the system for inlet flow velocities of 2.0, 1.0 and 0.5. From standard planar Couette flow NEMD simulations, the limiting zero shear rate shear viscosity for $\rho = 0.73$, $T = 1.0$ is $\eta = 1.6$. This gives R_e as 60, 30 and 15 for

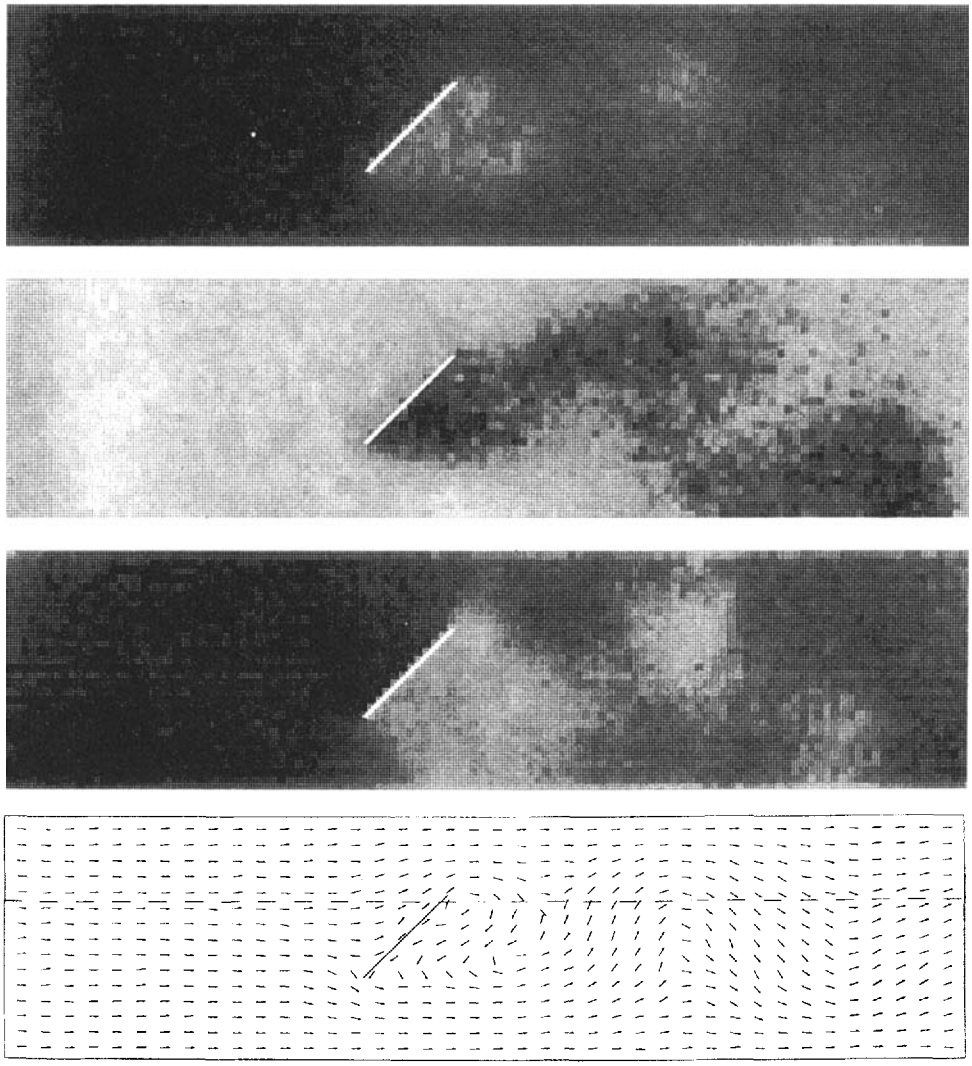

Figure 2 Continued. (c)

flow velocities of 2.0, 1.0 and 0.5 respectively. The Mach numbers corresponding to these velocities are not known exactly. However from the known Lennard-Jones triple point sound speed, $c = 5.5$, we can deduce that for our system the Mach numbers will be somewhat less than, 0.36, 0.18, 0.09, for the three flow velocities respectively. All the calculations reported in the following used a reduced time step of 0.003.

The velocity field of the system at different times of the simulation is shown in Figure 1. Each arrow represents the average local velocity for a cell, β. The averages are taken for all particles in each cell at every time step and these are in turn averaged over a period of 2000 time steps (i.e., 6 time units) to reduce the thermal fluctuations. The region shown in Figure 1(a)–(d) corresponds to half of the central region of the

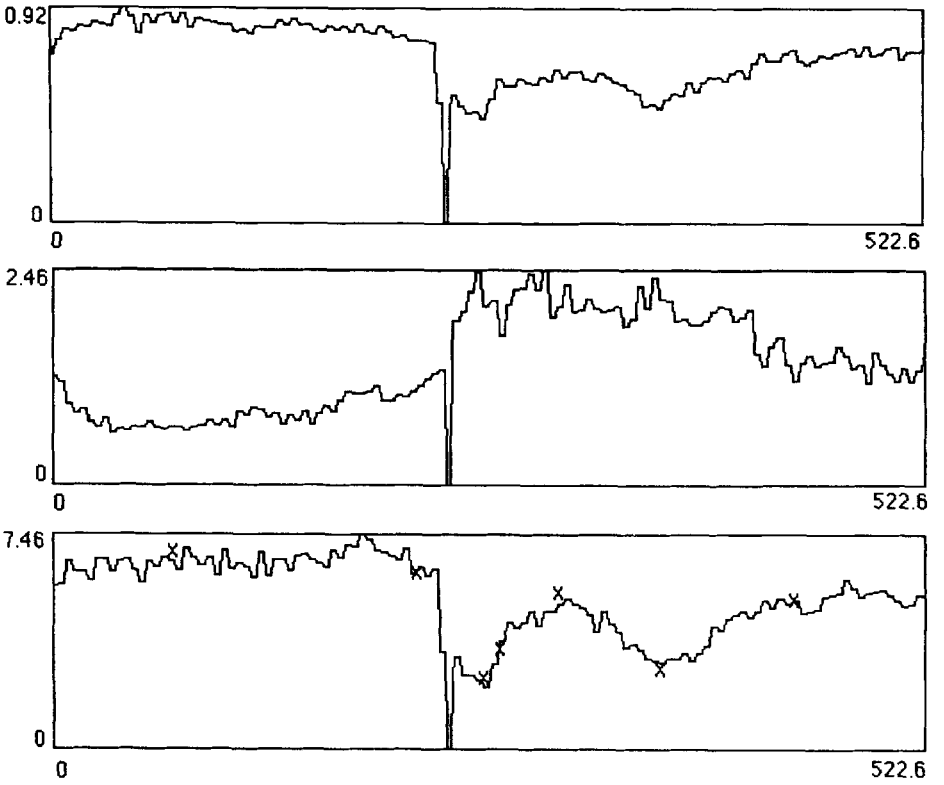

Figure 2 Continued. (d)

system ($0.25L_x \leqslant x < 0.75L_x, 0 \leqslant y \leqslant L_y$). The simulation was run for 62,000 time steps, corresponding to a total length of 186 time units. The flow was started abruptly after initial equilibration. At time $t = 42$, a vortex formed at the lower edge of the plate. At $t = 84$, the first vortex shed and travelled down stream while another vortex formed at the upper edge of the plate. The alternate vortex process continued so that

Table 1 The numerical values of thermodynamic variables at positions corresponding to the crosses in the pressure plot of Figure 2(d). x represents the x-coordinate of these positions on the ruled horizontal line indicated in Figure 2(c), ρ, T and P are the values of local density, temperature, and pressure at these positions. P_0 is the equilibrium pressure calculated from 224 particle simulation using the measured values of ρ and T.

x (σ)	ρ	T	P	P_0
71.9	0.8989	0.6823	6.53	6.82
217.8	0.7811	1.1458	6.37	6.24
256.9	0.4553	2.0470	2.16	2.25
266.7	0.6163	1.7251	3.80	3.91
301.6	0.6594	2.0470	5.02	5.50
362.6	0.4946	2.1242	3.02	2.76
442.0	0.7419	1.2102	5.15	5.35

Table 2 The thermodynamic properties of the system for flow velocity 2.0 at time $t = 186$ and flow velocity 0.5 at time $t = 252$, where the minimum, maximum and average values were taken over the 120×30 cells over a period of 2000 time steps.

V	ρ			T			P		
	Min	*Max*	*Ave*	*Min*	*Max*	*Ave*	*Min*	*Max*	*Ave*
2.0	0.452	0.997	0.730	0.44	3.27	1.30	2.13	8.17	5.35
0.5	0.473	0.816	0.730	0.64	1.49	0.94	2.13	5.33	4.19

at $t = 126$ we see that the two previous vortices have travelled down stream and a third one appears at the lower edge of the plate. A fourth vortex appeared at $t = 186$ at the upper edge of the plate.

Figure 1(e) shows the flow field for the rightmost 3/4 of the system (i.e., $x \geqslant 0.25L_x$, $0 \leqslant y \leqslant L_y$) at $t = 186$. A general feature of the flow is that it slows down in front of the plate but accelerates considerably in the area between the walls and the plate. Our numerical data show that the maximum local velocity is between 2 and 3 times of the inlet flow velocity for the system. This enhanced tip velocity is known to enhance the vortex shedding process compared to the free boundary case where the top and bottom walls are infinitely distant from the plate.

Figure 2 shows distributions of the density, temperature and pressure fields for a flow velocity of 2.0 at $t = 84$ and $t = 186$. The darker color corresponds to higher value of the quantity being graphed. We note the following general features from these distributions. The local thermodynamic variables show marked differences in front relative to behind the plate. In the areas in front and far downstream from the plate, the density, temperature and pressure are relatively smoothly distributed. Behind the plate, the distribution of local thermodynamic variables shows considerable structure. One can see from the accompanying flow direction plot, Figure 2(a), that the two regions of lower density and pressure correspond quite closely to the centres of the two vortices that are apparent in the flow. The temperature field shows a somewhat different structure with high temperature filaments emerging from both plate tips.

In the flow direction plot we can see a ruled horizontal line passing through the approximate centre of the top vortex. The accompanying plots in Figure 2(b) show the local values of density, temperature and pressure at locations along this ruled line.

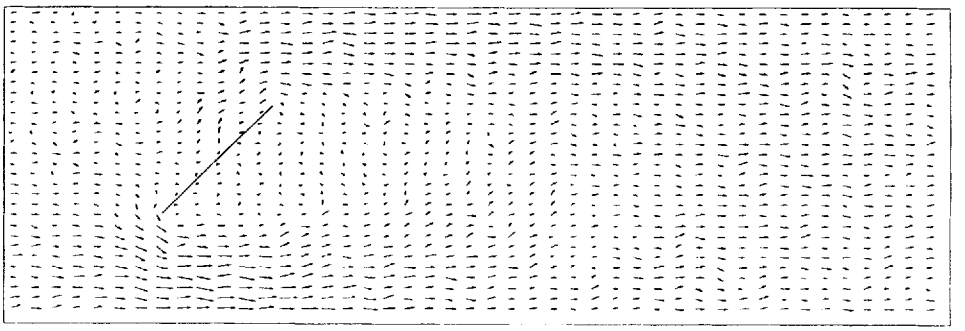

Figure 3 The velocity fields at the end of the simulation ($t = 252$) for flow velocity 0.5.

Again one can see that the centre of the top vortex is characterised by low density and pressure.

In Figure 2(c) and (d), we see the same sets of results as in Figure 2(a) and (b), but at a later time. The results seen in the two sets of figures are broadly similar. The local equation of state along the ruled line again shows lower values for the density and the pressure at the approximate centres of the vortices.

In the pressure plot we also show with crosses, values of the *equilibrium* pressure evaluated at the local temperature and density at that particular location. The corresponding numerical data are shown in Table 1. What we see is perhaps at first surprising. We see that even on this small scale where in terms of argon units the local hydrostatic pressure changes by tens of kilobars in distances of 100 Å, local thermodynamic equilibrium is satisfied within statistical uncertainties. These equation of state comparisons include data points within the shedding vortices.

At flow velocity 1.0, a vortex shedding process similar to the one at flow velocity 2.0 was observed. These were recorded but not shown here due to space limitations. The simulation was also run for 186 MD units. The first vortex appeared at about $t = 60$ at the lower edge of the plate. The second vortex appeared at about $t = 132$ at the upper edge as the first vortex travelled down stream. At the time when the simulation was terminated, the two vortices have travelled down stream and a third one was about to form at the bottom edge. It is worth noting that the rate of the vortex shedding is roughly half of the previous one, in proportion to the flow velocity.

For flow velocity 0.5, the simulation was run for 252 time units. The velocity field at the end of the run is shown in Figure 3, which is also the average over 2000 time steps. From the figure, it is apparent that there is no vortex formation in this case. The velocity field at various stages of the simulation were recorded but are not shown, as no vortices were observed. One notable feature for this low Reynolds number flow is that the local average velocity field is noisier, due to the relatively stronger thermal motion in comparison to the streaming motion. The density, temperature and pressure distribution at time $t = 252$ MD units for the case of flow velocity 0.5 are shown in Figure 4. A notable feature compared to the case of flow velocity 2.0, is that there are small differences in density and temperature on the two sides of the plate. The local state variables are relatively uniformly distributed.

To give some quantitative idea of the variation of local thermodynamic variables at the different flow velocities we show in Table 2 the density, temperature and pressure at the time of termination for the respective simulations. The minimum, maximum, and average refer to the corresponding variables taken over all the cells in the system. It is obvious from the table that as expected, the variation of thermodynamic variables is much smaller at the lower flow velocity.

The dependence of the drag coefficient on flow velocity is of some theoretical and practical interest. The drag coefficient, is defined for two dimensional systems as

$$C_d = \frac{F}{\frac{1}{2}\rho v^2 l} \tag{7}$$

where F is the force on the obstacle, ρ the density, v the flow velocity and l the characteristic length of the obstacle. For two dimensioanl flow past a plate, hydrodynamics predicts that the drag coefficients should decrease at low Reynolds number flattening out at higher Reynolds number [7]. The range of values of the Reynolds numbers accessible to molecular dynamics simulation is quite small as shown in

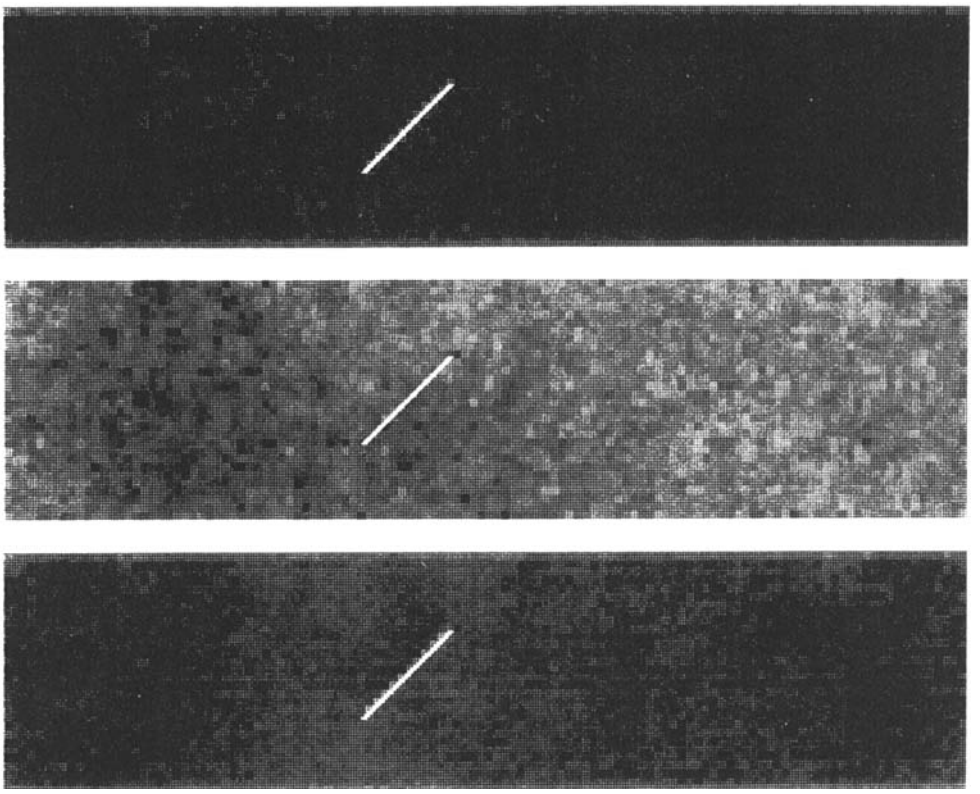

Figure 4 (a) The local density, temperature and pressure distributions corresponding to Figure 3. (b) Plots for the respective numerical values of the local distributions in Figure 3, along a horizontal line run across the center of the simulation box.

Figure 5. We note from the figure that in the limited range covered by our simulations, the drag coefficient decreases almost linearly with the Reynolds number.

DISCUSSION

We have refined the algorithms of Meiburg and of Rappaport for carrying out molecular dynamics simulations of "hydrodynamic" flows around obstacles. Our refinements improve the temperature and velocity stability of the inlet fluid stream.

Our results show that one can observe steady vortex shedding around a plate, in simulations involving $\sim 50{,}000$ particles. These techniques also allow the exploration of the fine details of local variations of the equation of state at a length scale which is much smaller than the characteristic radii of the vortices. The results show that within statistical uncertainties of $\sim 10\%$, the *equilibrium* equation of state correctly predicts the local pressure as a function of the local density and temperature. The postulate of local thermodynamic equilibrium is a remarkably accurate approximation for our system.

When translated into values for argon where ($\sigma \sim 3.405$ Å, $\varepsilon/k_B = \sim 120$ K and $m = \sim 40$ AMU) we note that a flow velocity of 1 in reduced units corresponds very

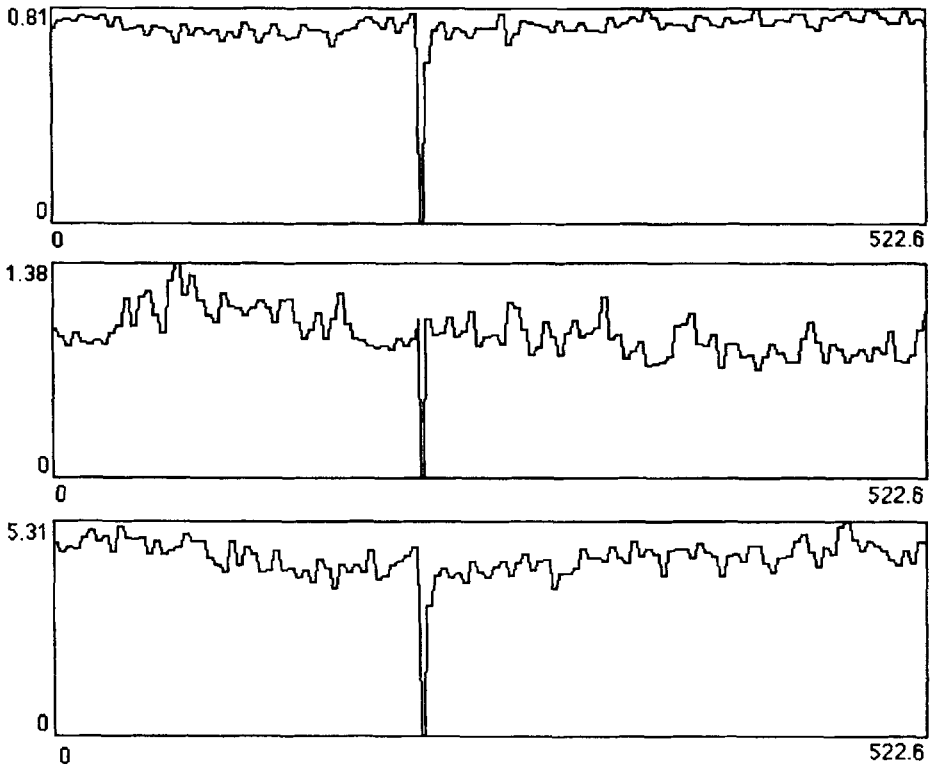

Figure 4 Continued. (b)

approximately to 150 m s^{-1}. Our simulations predict that if liquid argon at 120 K and 2 kilobars of pressure (note a reduced pressure of unity corresponds approximately to 420 bars in argon), is forced down a channel 400 Å wide at a velocity of 150 m s^{-1} past an obstacle 200 Å long, then vortices $\sim$ 50 Å in diameter will form in a down stream flow. The pressure drop inside these vortices will be of the order of a thousand atmospheres. In spite of these apparently "large" variations in thermodynamic parameters, local thermodynamic equilibrium holds to better than $\sim$ 10%.

The robustness of local thermodynamic equilibrium to these rapid and large changes is simply a manifestation of a fact that has been known from molecular dynamics simulations for decades. A computer simulation of a two dimensional system of 100 atoms, 30 Å on a side, will equilibrate in less than 2×10^{12} s, to a pressure that is within a couple of percent of the true equilibrium pressure.

The correspondence between the vortex location and the regions of low density and pressure can be understood from a simple mechanical argument. The rotational motion within a vortex will produce a centrifugal force which, when combined with the local hydrostatic pressure, will attempt to establish a local mechanical balance. This means that in regions of high vorticity, the hydrostatic pressure is likely to be lower than otherwise would be the case. (Note that uniform streaming motion makes no direct contribution to the hydrostatic pressure.) Regarding the density variation

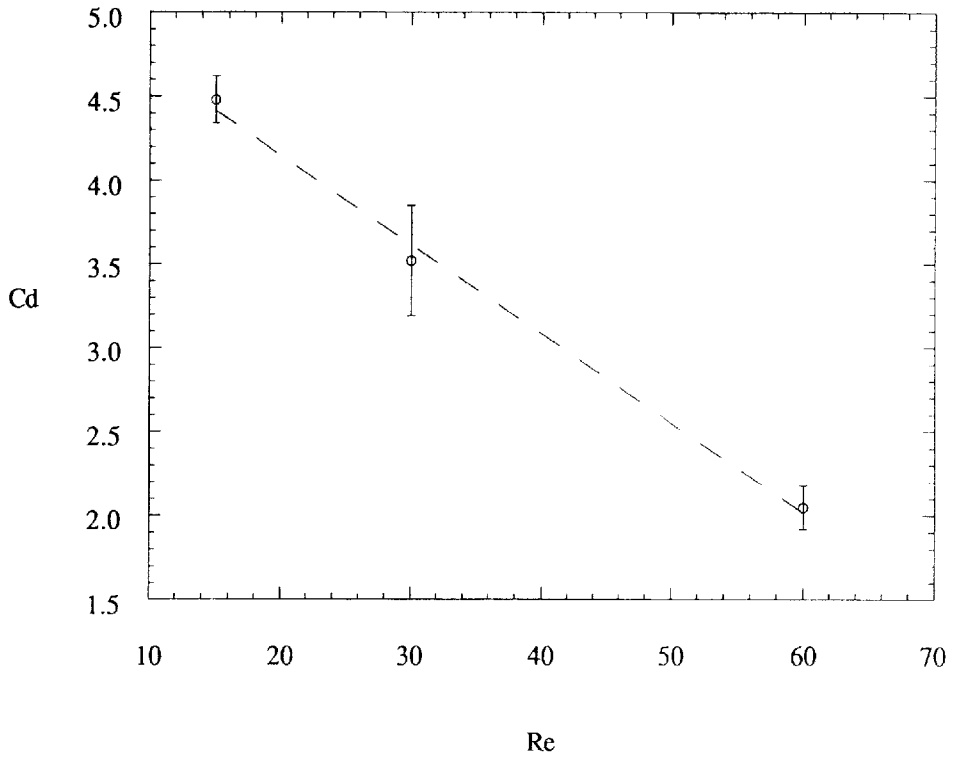

Figure 5 The calculated drag coefficient versus Reynolds number from the simulation.

within vortices, we would expect that the centrifugal force, acting on particles within a vortex should reduce the density compared to the surrounding fluid.

Acknowledgement

The authors would like to thank the Australian National University Supercomputer Facility for a generous grant of computer time.

References

[1] E. Meiburg, "Comparison of the molecular dynamics method and the direct simulation Monte Carlo technique for flows around simple geometries", *Phys. Fluids*, **29**, 3107 (1986).
[2] D.C. Rapaport, "Molecular-dynamics study of Rayleigh–Bénard convection", *Phys. Rev. Lett.*, **60**, 2480 (1988).
[3] D.C. Rapaport and E. Clementi, "Eddy formation in obstructed fluid flow: a molecular-dynamics study", *Phys. Rev. Lett.*, **57**, 695 (1986).
[4] M. Mareschal and E. Kestemont, "Experimental evidence for convective rolls in finite two-dimensional molecular models", *Nature*, **329**, 427 (1987).
[5] Enrico Clementi (ed), *Modern Techniques in Computational Chemistry, MOTECC-91*, p. 1031. ESCOM, Leiden (1991).
[6] D.J. Evans and G.P. Morriss, *Statistical Mechanics of Nonequilibrium Liquids*, p. 100. Academic Press, London (1990).
[7] See for example, J.C. Hunsaker and B.G. Rightmire, *Engineering Applications of Fluid Mechanics*, p. 198 McGraw-Hill, New York (1947).